1997

Small-scale cosmic microwave background observations at 8.4 GHz

Bruce Partridge
Haverford College, bpartrid@haverford.edu

Eric A. Richards

E. B. Fomalont

K. I. Kellermann

1997

Small-scale cosmic microwave background observations at 8.4 GHz

R. Bruce Partridge
Haverford College

Eric A. Richards

Edward B. Fomalont

K. I. Kellermann

THE ASTROPHYSICAL JOURNAL, 483:38–50, 1997 July 1

SMALL-SCALE COSMIC MICROWAVE BACKGROUND OBSERVATIONS AT 8.4 GHz

R. BRUCE PARTRIDGE
Haverford College, Haverford, PA 19041
ERIC A. RICHARDS
University of Virginia and National Radio Astronomy Observatory,[1] Charlottesville, VA 22903
EDWARD B. FOMALONT AND K. I. KELLERMAN
National Radio Astronomy Observatory,[1] Charlottesville, VA 22903
AND
ROGIER A. WINDHORST
Department of Physics and Astronomy, Arizona State University, Tempe, AZ 85287-1504
Received 1996 September 10; accepted 1997 January 16

ABSTRACT

We have used the Very Large Array (VLA) of the National Radio Astronomy Observatory at 8.44 GHz to image a ~ 40 arcmin^2 field with an uprecedented rms sensitivity of 1.5 μJy. After correcting for the effects of discrete foreground radio sources, we examined this most sensitive microwave image of the sky for fluctuations in the cosmic microwave background radiation (CBR). At the 6″ resolution of our VLA map, $\Delta T/T \approx (0.7 \pm 0.8) \times 10^{-4}$, with an upper limit of 1.3×10^{-4} at 95% confidence. At 1′ resolution, we measure a fluctuation amplitude of $\Delta T/T = (1.2 \pm 1.4) \times 10^{-5}$. We also report on our observations of the linear and circular polarization of the CBR for which we derive upper limits (at 95% confidence) of $\Delta T/T \leq 1.1 \times 10^{-5}$ and $\Delta T/T \leq 1.6 \times 10^{-5}$, respectively, on an angular scale of 1′.

Subject headings: cosmic microwave background — cosmology: observations — radio continuum: general

1. VERY SMALL-SCALE COSMIC MICROWAVE BACKGROUND RADIATION ANISOTROPIES: ORIGINS AND OBSERVATIONS

Much attention, both theoretical and observational, has been devoted to cosmic microwave background radiation (CBR) fluctuations on scales of 1° and larger, especially since the first detection of these anisotropies by the *COBE* Differential Microwave Radiometer team (Smoot et al. 1992). Because angular variations in the CBR on these large scales are primordial, originating at $z \gtrsim 1000$, such observations provide a powerful test of virtually all theories of the formation and cosmological evolution of large-scale structure (see White, Silk, & Scott 1994 or Partridge 1995 for reviews). However, on angular scales below $\sim 7'$, these primordial fluctuations are smoothed away because of the extended timescale over which cosmological recombination took place (e.g., Vittorio & Silk 1984). Thus, any primordial fluctuations on the angular scales accessible to the Very Large Array (VLA) (typically a few arcmin or below) are expected to be vanishingly small. Observations on arcminute scales and below instead offer a means to probe a wide variety of astrophysical processes that occur at later epochs (at $z \ll 1000$). Fluctuations introduced into the CBR well after the epoch of recombination are referred to as *secondary fluctuations*; observations on $\sim 1'$ scale offer a clean test for any such secondary fluctuations. For $z \lesssim 10$, and reasonable cosmological models, the angular scales we probe, 0.′1–1′, sample 30–300 kpc structures (i.e., protogalaxies, protogroups, or protoclusters).

[1] The National Radio Astronomy Observatory is operated by Associated Universities, Inc., under cooperative agreement with the National Science Foundation.

1.1. *Secondary Fluctuations in the CBR*

Several models have been proposed to generate secondary fluctuations. Reionization of the intergalactic medium by a large injection of energy after recombination has been investigated by a number of authors (Ostriker & Cowie 1981; Ikeuchi 1981; Vishniac 1987; Tegmark et al. 1994). Possible sources of energy input in these scenarios include large ionizing radiation fields from a first generation of massive stars, quasars, and/or active galactic nuclei. A reionized universe would introduce fluctuations via the Vishniac effect (Vishniac 1987), which is a second-order Doppler shift imprinted on the surface of last scattering by the bulk motions of matter at the time of reionization. Fluctuation amplitudes on the order of $\Delta T/T \approx 10^{-5}$ are predicted. Another possibility, although less conventional, is the introduction of anisotropies from relativistic cosmic strings (Bouchet, Bennett, & Stebbins 1988; Hindmarsh 1993; Moessner, Perivolaropoulos, & Brandenberger 1994), again on arcsecond scales.

Recently, Loeb (1996) has shown that bremsstrahlung emission from Lyα clouds will produce microwave fluctuations with amplitudes $\Delta T/T$ in the 10^{-6} to 10^{-5} range.

Perhaps the most investigated method of introducing CBR fluctuations is through the inverse Compton scattering of the CBR photons off very hot electrons, the Sunyaev-Zel'dovich (SZ) effect (Sunyaev & Zel'dovich 1972). One of the possible sources for a large reservoir of scattering electrons is Zel'dovich pancakes, which are massive metagalactic progenitors of present superclusters that may have formed from asymmetrical density perturbations before recombination. Fluctuation amplitudes are expected to be of order 10^{-6} to 10^{-7} in $\Delta T/T$ and on somewhat larger scales than we probe (see, e.g., Rephaeli 1993; SubbaRao et al. 1994). Next, there are the SZ signals

from relatively nearby clusters of galaxies, which have been unambiguously observed in exceptionally rich clusters such as A2218 and 0016+16 on scales of a few arcminutes and at levels of several hundred μK (Birkinshaw & Hughes 1994; Herbig et al. 1995; Wilbanks et al. 1995; Carlstrom et al. 1996a, 1996b; Grainge et al. 1996). A background of higher redshift clusters would also produce such anisotropies, since the observed amplitude of the SZ effect is independent of distance. Such scenarios have been investigated by Schaeffer & Silk (1988); Cole & Kaiser (1988); Markevich et al. (1992, 1994); Makino & Suto (1993); and Colafrancesco et al. (1994). These authors predict $\Delta T/T \approx 10^{-5}$ for some of the more optimistic models on scales of 1′. A review of these and related papers is given by Rephaeli (1995).

A final source of fluctuations in the microwave sky, of less interest for studies of the early universe, is the contribution by foreground radio sources. First, thermal bremsstrahlung, dust emission, and synchrotron radiation from our Galaxy all vary across the sky. However, in principle, these effects can be separated out from extragalactic CBR fluctuations by observations at different frequencies and angular scales (see Banday & Wolfendale 1991; Brandt et al. 1994; Partridge 1995). Also, there is the problem of confusion by faint, nonthermal radio sources. Detailed modeling by Franceschini et al. (1989) shows that these extragalactic sources can mimic genuine CBR anisotropies up to the level of $\Delta T/T \approx 3 \times 10^{-5}$ for our observing wavelength and in the range of angular scales we explore. Our ability to model successfully the effects of these discrete sources in our maps ultimately determines the sensitivity of our search for secondary CBR fluctuations.

1.2. *Previous Observations*

With the exception of the 1.3 mm observation of Kreysa & Chini (1989), all measurements of, or upper limits on, CBR fluctuations on subarcminute scales have been made using interferometric (aperture synthesis) techniques. The first interferometric observations (Martin, Partridge, & Rood 1980) employed a wide spacing, three element interferometer and were, as a consequence, quite insensitive. The 27 antenna VLA offers much better sensitivity and was used in searches for CBR fluctuations, both total intensity (Fomalont et al. 1984; Knoke et al. 1984) and polarized (Partridge, Nowakowski, & Martin 1988). In all this early and subsequent work, correction for point sources and their sidelobe contributions played a crucial role.

The addition of low-noise 8.4 GHz receivers to the VLA in 1989 allowed both more sensitive observations and a reduction of the effect of foreground radio sources, whose contribution to brightness temperature fluctuations scales approximately as $\nu^{-2.7}$ for typical synchrotron emitters. Limits on CBR fluctuations on a range of angular scales from 10″ to 80″ were established at 8.4 GHz ($\lambda = 3.6$ cm) by Fomalont et al. (1993); these results are summarized in Table 1, along with some other results either at different wavelengths or on angular scales near that range. We note that the sensitivity (in $\Delta T/T$) of the VLA measurements on a 1′ scale is comparable to the *COBE* measurement of Smoot et al. (1992) on a 7° scale and to the best filled-aperture results on somewhat larger angular scales (Readhead et al. 1989), which give $\Delta T/T \leq 1.7 \times 10^{-5}$.

Very similar work carried out at the Australia Telescope Compact Array by Subrahmanyan et al. (1993) gives results on arcminute scales very similar to those obtained at the VLA; their synthesized beam size is ∼2′ FWHM, and at this scale, the 95% confidence level upper limit on $\Delta T/T$ fluctuations is given as 9×10^{-6}. This estimate is based on only eight to 10 samples within their primary beam solid angle. The IRAM interferometer has also been used (Radford 1993) to set limits on $\Delta T/T$ at millimeter wavelengths (see Table 1).

TABLE 1

PREVIOUS OBSERVATIONAL RESULTS, $\theta \lesssim 2'$

Resolution (arcsec)	λ (cm)	Stokes Parameter	$\Delta T/T$[a] ($\times 10^{-5}$)	Reference
6	6	I	<320	1
5.3	2	I	<63	2
30[b]	0.13	I	<26	3
10	0.34	I	<9	4
10	3.6	I	<7.2	5
18	3.6	I	<5.8	5
30	3.6	I	<4.0	5
60	3.6	I	<2.3	5
80	3.6	I	<1.9	5
10	3.6	V	<5.9	5
30	3.6	V	<3.6	5
80	3.6	V	<2.2	5
10	3.6	$\sqrt{U^2+Q^2}$	<6.9	5
30	3.6	$\sqrt{U^2+Q^2}$	<3.3	5
80	3.6	$\sqrt{U^2+Q^2}$	<2.1	5
∼120	3.5	I	<0.9	6

[a] At 95% confidence.

[b] Beam-switch angle.

REFERENCES.—(1)Knoke et al. 1984; (2) Hogan & Partridge 1988; (3) Kreysa & Chini 1989; (4) Radford 1993; (5) Fomalont et al. 1993; (6) Subrahmanyan et al. 1993.

1.3. *Outline of This Paper*

Section 2 outlines our observational techniques and the construction of images at various angular resolutions (some further details are presented by Kellermann et al. 1996, hereafter Paper I). We then discuss the techniques we employed to remove discrete foreground radio sources detected in these images. In § 3, we treat the contribution of atmospheric and instrumental noise and the calculation of the excess variance in the maps produced by either CBR fluctuations or foreground radio sources too weak to be detected individually in our 8.44 GHz radio images. We also describe Monte Carlo simulations designed to examine the effect of both weak foreground sources and some systematics on the noise properties of our VLA maps. In § 4, we set limits on CBR fluctuations on various angular scales, both total intensity and polarized, and analyze the effect on these limits of our assumptions about the weak ($S < 7$ μJy) source counts and of one particular, extended, negative feature in our map. In the final section, we compare our results and upper limits with some of the models discussed above and draw conclusions about the nature of primary and secondary CBR fluctuations, reionization scenarios, and the epoch of cluster and large-scale structure formation.

2. OBSERVATIONS AND CONSTRUCTION OF THE 3.6 cm RADIO IMAGES

The results presented here are based on VLA observations of a single field centered at (J2000) R.A. = $13^h12^m17^s.4$ and decl. = +42°38′06″. This radio field included one of the survey areas of the Medium Deep Survey (MDS) made by the *Hubble Space Telescope* (Windhorst et al. 1994, 1995). This particular MDS field was

selected because it was free of "bright" ($S_{3.6\,\mathrm{cm}} \geq 1$ mJy) radio sources.

2.1. *Observations*

The center frequency of our observations was 8.44 GHz. We used an effective bandwidth of 100 MHz in each of two orthogonal circular polarizations. From 1993 October through 1994 January, we collected 84 hr of good-quality data with the VLA in its most compact D configuration. An additional 75 hr were obtained in the C configuration from 1994 November through 1995 January. The approximate FWHMs of the synthesized VLA beam in these two configurations are $\theta_{1/2} = 10''$ and $3''$, respectively. The FWHM of the final map, which combined all the observations, is $\theta_{1/2} \approx 6''$. The field of view of the VLA, determined by the full width of the primary beams of the antennas of the array, was $312''$ in diameter at half-power, or $444''$ out to the first nulls of the beam. The VLA primary beam shape at 8.44 GHz is given in Windhorst et al. (1993a). All four Stokes parameters were observed in both configurations.

In all our runs, observations of about 27 minute duration of the 13^h field were alternated with 2–3 minute observations of the calibrator source 1244+408, which we used as a phase reference. Our flux and polarization calibration was based on 3C 286, for which we assumed a flux density of 5.19 Jy and 10% linear polarization at position angle 30°.5. This value is based on the flux density scale of Baars et al. (1977). Residual variations in the gain of individual correlators were $\lesssim 3\%$ after calibration, and residual phase fluctuations were almost always $\leq 5°$. The *u-v* data were edited to remove occasional interference and data associated with atennas shadowed by other antennas in the array; less than 1% of our data were dropped for these reasons. However, because of inclement weather, including snow, during four of our 27 individual observing runs, we did not use another 30 hr of data out of 190 total hr. Finally we examined the individual antenna gains over 30 minute intervals and used these values to give a proper weighting to our visibility data. We weighted the visibilities produced by each pair of antennas in inverse proportion to the product of the rms of the signals from the two antennas within that time period.

2.2. *Images*

As described in Fomalont et al. (1993), we constructed both a *sum* and a *difference* image, using natural weighting and $0''.667$ cells for each; these are shown in Figure 1. The sum image contains all the (unflagged) *u-v* data from all days and in both configurations. The difference image was constructed by dividing both the C and D configuration observations into two independent data sets. The two sets were selected to have roughly equal numbers of days of observation randomly interspersed through both observing runs and to sample the duration of the runs similarly in order to obtain similar *u-v* coverage, receiver gains, and phase stability. These two independent data sets were imaged with identical parameters, and the images were then subtracted. In this difference image, any correlated signals, including both foreground sources and CBR fluctuations, will in principle cancel out (except for variable radio sources), leaving only instrument noise. The difference map is used as one measure of the instrument noise in the corresponding sum map (see Fomalont et al. 1993 for further discussion). The rms noise for the difference image formed in this way is 1.56 μJy.

In addition to images made at the full $6''$ resolution of our observations, we constructed sum and difference images at lower resolution by convolving a Gaussian weighting function with our visibility data, thus weighting down the longer baseline spacings and broadening the synthesized beam. We constructed tapered images with approximately $10''$, $18''$, $30''$, $60''$, and $80''$ resolution (FWHM); the $18''$ image is shown in Figure 1. Like the full-resolution image, these tapered images were heavily oversampled, using $1''.33$, $2''.67$, $4''$, $6''$, and $6''$ pixels, respectively.

We also constructed similar full-resolution images and tapered, lower resolution, images in the other three Stokes parameters, Q, U, and V. These are used in § 4.2 to set limits on polarized fluctuations in the CBR. In addition, the Stokes V images provide useful estimates of the instrument noise, since (1) they employ the same data as the total power maps (i.e., RR − LL vs. RR + LL) and (2) neither CBR fluctuations nor foreground radio sources are expected to contribute significantly to the sky variance in Stokes V maps, since neither is circularly polarized. For our full-resolution V map, the rms noise was 1.57 μJy, very close to the value obtained for the full-resolution difference map.

We also constructed a linearly polarized image by adding the Q and U images in quadrature: $P = (Q^2 + U^2)^{1/2}$. We examined all these polarized images carefully to look for discrete sources. None of the polarized images showed residual peaks at the positions of the strong sources seen in the total power image. All subsequent analyses were therefore conducted on the polarized images without either cleaning or source removal.

2.3. *Removal of Bright Foreground Radio Sources*

Our interest is in small-scale fluctuations in the CBR. Hence, the fluctuations introduced into our image by foreground radio sources are contaminants we wish to eliminate or minimize.

We begin with "bright" foreground sources, those discussed in Paper I. These are the sources with peak flux in the $6''$ resolution image of ≥ 7.0 μJy (or 4.7 σ).[2] Forty-six sources above this threshold were found in our sum image, of which 39 appear in the complete catalog (Kellerman et al. 1996) of sources lying within the 10% level of the primary beam. Each of the 46 "bright" sources was removed using the technique developed by Fomalont et al. (1993). We found the position of each source, then performed the CLEAN operation in a $3''.3 \times 3''.3$ box around each. We cleaned each source to a predetermined level of 1.5 μJy (~ 1 σ). The visibility function formed from these 46 sets of clean components was then subtracted from the *raw* visibility data to provide a new set of *corrected* visibility data. When these corrected visibilities are Fourier transformed and imaged, the resulting images are free of all the bright sources *and their sidelobes* at all resolutions.

Note, however, that each of these bright sources has been truncated at the 1 σ level. The corrected image thus contains remnant "stumps" of these 46 sources at the 1.5 μJy level, noise, and, more important, discrete sources with $S_i < 7$ μJy (and hence not part of the complete sample). The residual effects of both the bright sources and weaker sources will be discussed further in § 3.3.

[2] The image used by Kellermann et al. (1996) to search for sources is heavily cleaned, unlike the image discussed here. As a consequence, the rms is $\sim 5\%$ lower, at 1.49 μJy.

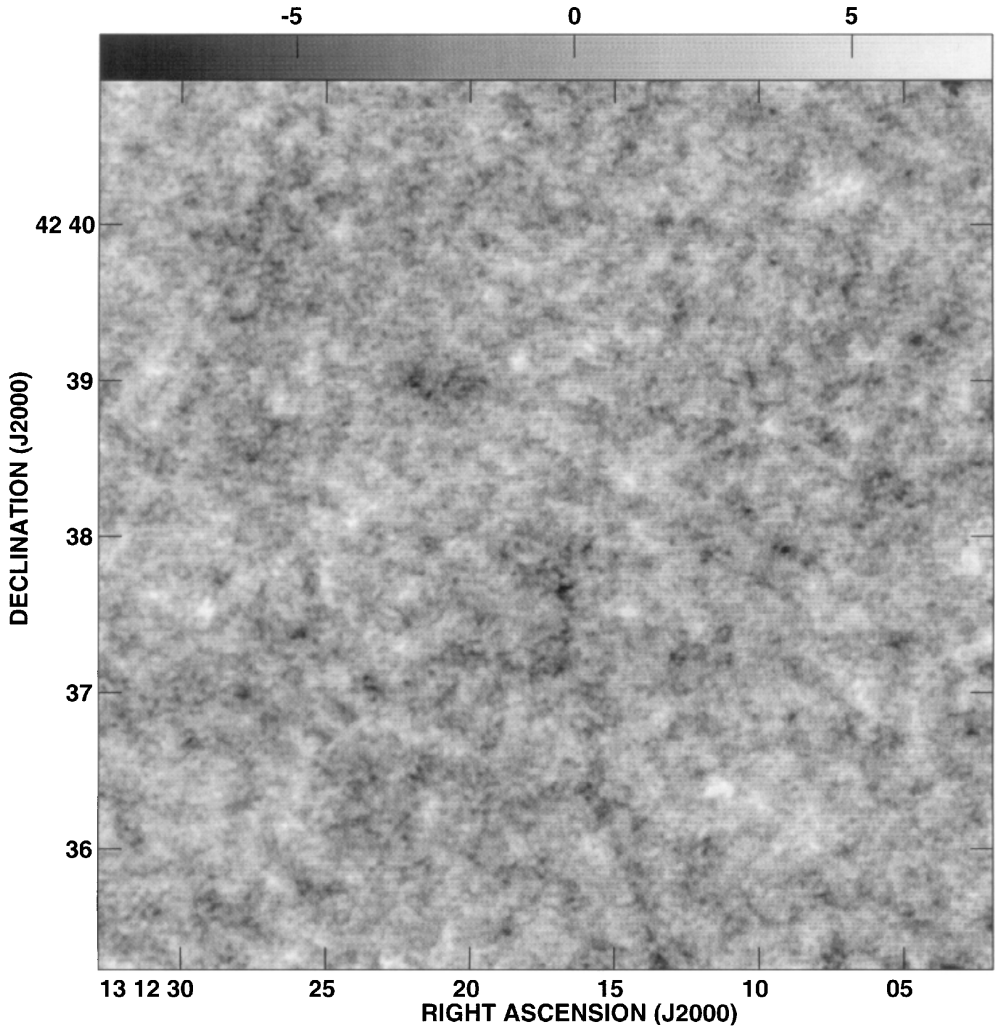

FIG. 1*a*

FIG. 1.—VLA images made at 8.44 GHz. (*a*) The *sum* image, at full 6″ resolution. Bright sources and their sidelobes have been removed, as detailed in § 2.3. (*b*) The corresponding *difference* image at 6″ resolution. (*c*) A tapered sum image at 18″ resolution. The possible Sunyaev-Zel'dovich feature discussed in § 4.3 is the vertical, double-lobed structure at $13^h12^m17^s$ and $+42°37'.5$.

Finally, both sum and difference images were constructed from these corrected visibility data. The difference image constructed from the corrected visibility functions provides us with our primary estimate of the instrumental and sky noise in our image: 1.56 μJy rms.

3. FURTHER CORRECTIONS

The sum image made from the corrected visibilities still contains weak foreground radio sources (below our 7.0 μJy threshold), instrumental and atmospheric noise, and possibly other instrumental artifacts. All these must be estimated before we can calculate appropriate measures of, or upper limits on, CBR fluctuations from our observations.

3.1. *Instrumental and Atmospheric Noise*

For reasons discussed by Fomalont et al. (1993), the difference image constructed from the corrected visibilities provides an accurate and correct measure of the instrumental noise, including noise introduced into the data by microwave emission from the Earth's atmosphere.

Another estimate, however, is provided by the outer regions of the sum image, as first noted by Martin et al. (1980). At large radial distances from the image center, the primary beam response of the VLA antennas falls close to zero (<3% in the first sidelobe and beyond). Thus, the amplitude of any fluctuations in the microwave sky—whether from CBR anisotropies or foreground sources—is reduced essentially to zero. The instrument noise, however, is in principle spread uniformly across both the sum and difference maps (see Knoke et al. 1984; Fomalont et al. 1993). As in Fomalont et al. (1993), we also allow for the possibility of a (small) radially dependent contribution from possible uncorrelated calibration errors and other artifacts, written as $\sigma_u(\theta)$, where θ is the distance in arcseconds from the image center. We may thus write for the expected variance in the difference image

$$\sigma_d^2(\theta) = \sigma_n^2 + \sigma_u^2(\theta) , \quad (1)$$

where σ_n is the instrumental noise.

For the *sum* image, we expect additional variance $\sigma_e^2(\theta)$ near the map center, where the primary beam response is large, contributed by both discrete foreground sources and, possibly, CBR anisotropies:

$$\sigma_s^2 = \sigma_d^2(\theta) + \sigma_e^2(\theta) . \quad (2)$$

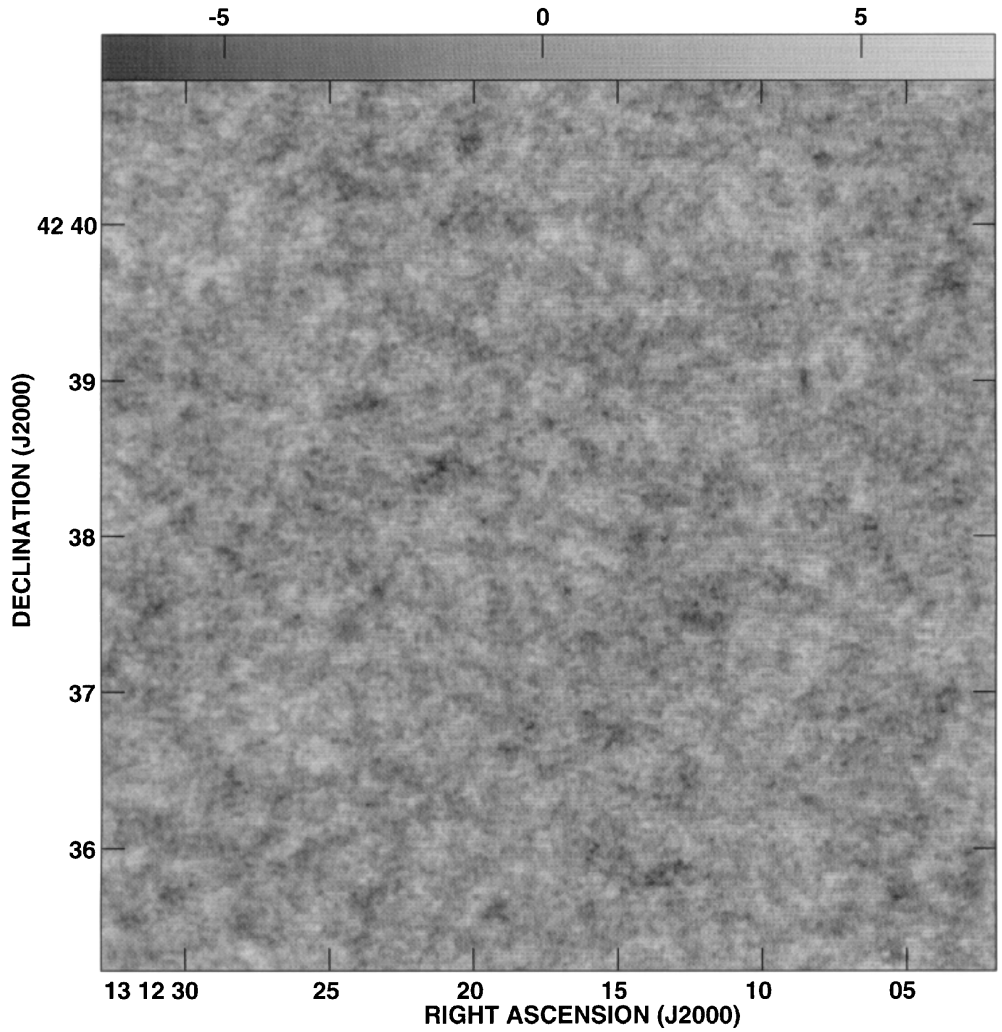

FIG. 1*b*

For an ideal experiment, with no low-level sidelobes of the synthesized beam, the excess variance, $\sigma_e^2(\theta)$, could be simply expressed as

$$\sigma_e^2(\theta) = P^2(\theta)\sigma_{\rm sky}^2 , \quad (3)$$

where $P(\theta)$ is the primary-beam response of the VLA and $\sigma_{\rm sky}^2$ is the total variance of the microwave sky at the resolution of our observation.

Because neither the sum nor difference images were heavily cleaned, some of the flux of each source in the image is scattered into sidelobes that can extend beyond the solid angle of the primary beam. This effect will be larger for the tapered, low-resolution maps because fewer independent pixels fit within the primary beam. The result is a slight broadening of the expected pattern of the excess variance, compared with that expected from the primary beam response alone. We take this effect into account in calculating a corrected value of the square of the primary beam response.

The variances for the sum and difference images for our field are shown in columns (4) and (5) of Table 2. These were calculated for a series of concentric rings, each of 100″ thickness, centered at the image center. We also give, in column (2), $\overline{P^2}(\theta)$, the value of the square of the primary beam

TABLE 2

VARIANCE AT 6″ RESOLUTION

Ring Radii (arcsec) (1)	$\overline{P^2}(\theta)$ (2)	Number of Beams, N (3)	σ_s^2 (μJy^2) (4)	σ_d^2 (μJy^2) (5)	σ_e^2 (μJy^2) (6)
0–100.....	0.78	699	3.22	2.39	0.77 ± 0.17
100–200.....	0.27	2096	3.04	2.44	0.59 ± 0.09
200–300.....	0.03	3494	2.61	2.48	0.16 ± 0.06
300–400.....	0.01	4891	2.59	2.48	0.14 ± 0.05
400–500.....	0.02	6289	2.50	2.47	0.05 ± 0.05
500–600.....	0.01	7685	2.47	2.42	0.02 ± 0.04
600–700.....	0.00	8766	2.60	2.48	0.15 ± 0.04
Average $\bar{\sigma}_d^2$				2.451 ± 0.014	

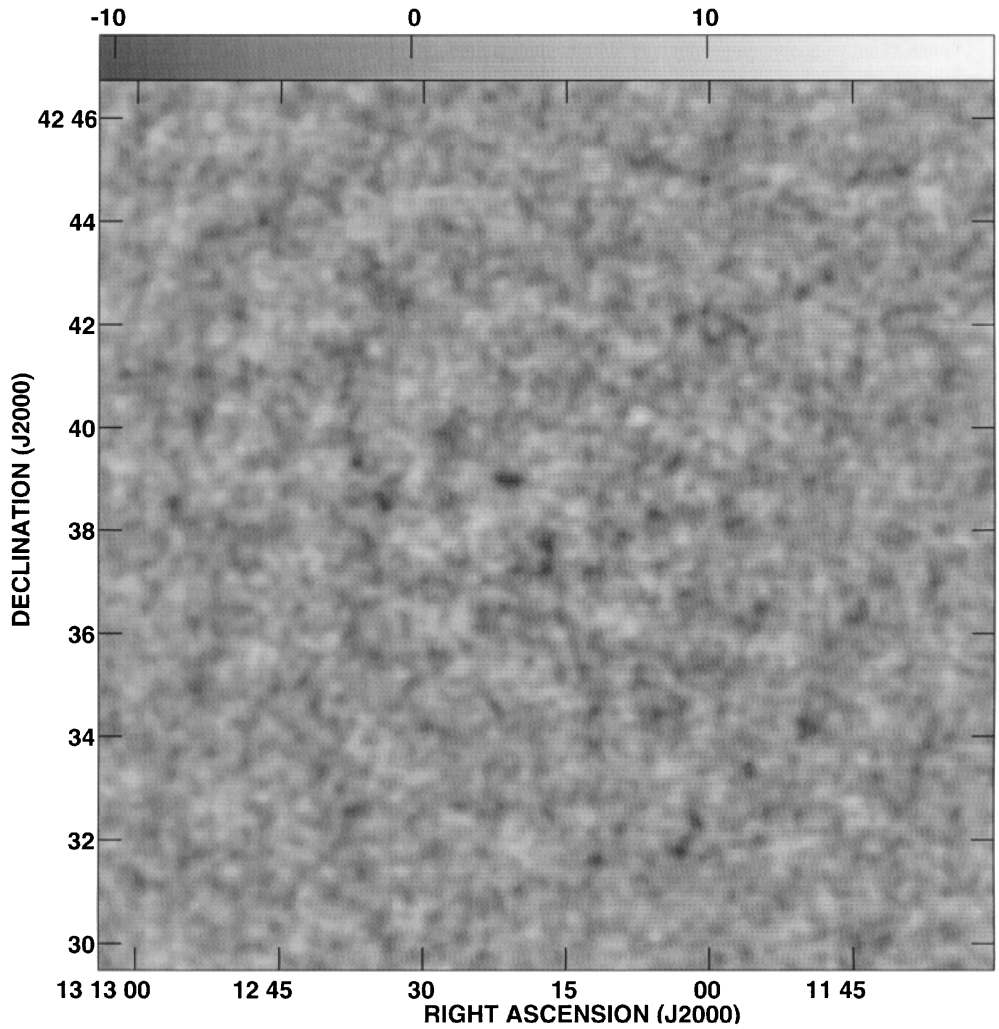

FIG. 1*c*

response averaged over each radial ring and corrected for the small effect mentioned in the paragraph above. As we expect, $\overline{P^2}(\theta)$ is appreciably different from zero only in the inner two rings. Our measurements show that σ_d^2 is essentially independent of distance θ from the map center; thus, $\sigma_u^2(\theta)$ appears to be negligibly small. Consequently, we give in the last line of Table 2 the average variance $\overline{\sigma}_d^2$, determined from all rings of the difference image, and the standard deviation of its mean, Δ_d. We use $\overline{\sigma}_d^2$ to evaluate the excess variance σ_e^2 in each ring; these values are shown in column (6) of Table 2. The errors in column (6) are calculated as

$$[2(\sigma_s^2)^2/N + \Delta_d^2]^{1/2}\,, \tag{4}$$

where N is the number of independent beam solid angles in each ring (col. [3]).

Tables 3 and 4 present similar information for tapered, lower resolution, images. For the lowest resolution (30″, 60″, and 80″) images, we used rings of 200″ thickness in order to obtain a reasonable number of independent samples in each ring.

As the synthesized beam size increases, so does $\bar{\sigma}_d^2$. The values for $\bar{\sigma}_d^2$ for maps at 10″, 18″, 30″, 60″, and 80″ resolution were, respectively, 3.22 ± 0.037, 5.92 ± 0.12, 13.03 ± 0.34, 43.1 ± 1.9, and 100 ± 8, in μJy^2. Recall that tapering VLA images effectively downweights data from longer baselines; thus by tapering we are throwing away some data (especially data from the C configuration runs). While the rms noise per synthesized beam increases, the limit on surface brightness is nevertheless improved, since it varies as $\Omega^{-1} \propto \theta^{-2}$.

3.2. *Modeling Weak Sources*

Some of the excess variance observed near the centers of sum images is produced by foreground radio sources that lie below our 7.0 μJy threshold for reliable detection and removal. To determine the effect of these weak sources, we performed a Monte Carlo analysis of the radio population in our field. We began by constructing a number count versus flux density relation for the brighter sources as cataloged in Paper I. We found 39 sources with flux densities ranging from 7 to $\sim$700 μJy within 275″ of the map center; this constitutes the complete radio catalog given in Paper I. The best-fitting, maximum-likelihood estimate for the integral source count law for these sources is

$$N(\geq S) = (17 \pm 2)S^{-1.2 \pm 0.2}\ \text{arcmin}^{-2}\,. \tag{5}$$

This relation agrees well with the integral source count found in Windhorst et al. (1993a) for the same observing frequency and flux density range: $(19 \pm 3)S^{-1.3 \pm 0.2}$ arcmin^{-2}. In Paper I, we present a detailed description of the methods used to determine relation (5).

TABLE 3

VARIANCE AT 10″ AND 18″ RESOLUTION

RING RADII (arcsec) (1)	$\overline{P^2}(\theta)$ (2)	10″ VARIANCE (μJy^2) N (3)	σ_s^2 (4)	σ_e^2 (5)	18″ VARIANCE (μJy^2) N (6)	σ_s^2 (7)	σ_e^2 (8)
0–100	0.78	287	4.97	1.75 ± 0.42	88	11.66	5.74 ± 1.76
100–200	0.27	860	4.58	1.36 ± 0.22	265	9.92	4.00 ± 0.87
200–300	0.03	1433	3.59	0.37 ± 0.14	441	6.85	0.93 ± 0.48
300–400	0.01	2006	3.58	0.36 ± 0.12	618	7.19	1.27 ± 0.43
400–500	0.02	2580	3.33	0.11 ± 0.10	794	6.30	0.38 ± 0.34
500–600	0.01	3153	3.31	0.09 ± 0.09	971	6.33	0.41 ± 0.31
600–700	0.00	3595	3.52	0.30 ± 0.09	1147	6.58	0.66 ± 0.30
700–800	0.00	...	...	...	1324	6.39	0.47 ± 0.28
800–900	0.00	...	...	...	1500	6.44	0.52 ± 0.26
900–1000.....	0.00	...	...	...	1677	6.47	0.55 ± 0.25

3.3. *Determining the Contribution from Weak Sources*

Since the source counts down to 7 μJy are fairly well determined (see the discussion in Windhorst et al. 1993b), we can extrapolate them to somewhat lower values of the flux density (typically 0.1 μJy). We then randomly populated a field with radio sources in the flux density range 0.1–700 μJy, with relative numbers as given by equation (5) above. We next added noise at an appropriate level (1.56 μJy rms for a full-resolution image). These simulated images were then analyzed in the same fashion as our real sky images.

In particular, we felt it prudent to scatter bright (7–700 μJy), as well as fainter, radio sources in our simulated images and then to subtract these bright sources from the simulated images with the identical technique we used for the actual sky images. Thus, any systematics resulting from

TABLE 4

VARIANCE AT 30″, 60″, AND 80″ RESOLUTION

RING RADII (arcsec) (1)	$\overline{P^2}\theta$ (2)	30″ VARIANCE (μJy^2) σ_s^2 (3)	σ_e^2 (4)	60″ VARIANCE (μJy^2) σ_s^2 (5)	σ_e^2 (6)	80″ VARIANCE (μJy^2) σ_s^2 (7)	σ_e^2 (8)
0–200	0.40	25.39	12.36 ± 3.37	75.0	31.9 ± 18.0	219	119 ± 72
200–400	0.01	16.66	3.63 ± 1.31	51.8	8.7 ± 7.4	148	48 ± 29
400–600	0.02	13.87	0.84 ± 0.89	39.9	-3.2 ± 4.7	122	22 ± 20
600–800	0.00	14.21	1.18 ± 0.79	39.5	-3.6 ± 4.0	115	15 ± 16
800–1000.....	0.00	14.31	1.28 ± 0.72	43.8	0.7 ± 4.0	125	25 ± 16
1000–1200.....	0.00	...	...	45.2	2.1 ± 3.8	122	22 ± 14
1200–1400.....	0.00	...	...	...	...	109	9 ± 13

TABLE 5

EXCESS, WEAK SOURCE, AND RESIDUAL VARIANCES

NOMINAL RESOLUTION (1)	RING RADII 0″–100″ σ_e^2 (2)	σ_w^2 (3)	σ_r^2 (4)	100″–200″ σ_e^2 (5)	σ_w^2 (6)	σ_r^2 (7)	200″–700″ σ_e^2 (8)	σ_w^2 (9)	σ_r^2 (10)
6″.....	0.77 ± 0.17	0.60 ± 0.11	0.17 ± 0.20	0.59 ± 0.09	0.29 ± 0.06	0.30 ± 0.11	0.10 ± 0.03	0.02 ± 0.01	0.08 ± 0.03
10″.....	1.75 ± 0.42	1.29 ± 0.23	0.46 ± 0.48	1.36 ± 0.22	0.66 ± 0.15	0.70 ± 0.27	0.25 ± 0.06	0.07 ± 0.05	0.18 ± 0.08
18″.....	5.74 ± 1.76	3.65 ± 0.63	2.09 ± 1.87	4.00 ± 0.87	1.96 ± 0.59	2.04 ± 1.05	0.73 ± 0.17	0.21 ± 0.13	0.52 ± 0.21

TABLE 6

EXCESS, WEAK SOURCE, AND RESIDUAL VARIANCES

NOMINAL RESOLUTION (1)	RING RADII 0″–200″ σ_e^2 (2)	σ_w^2 (3)	σ_r^2 (4)	200″–1000″ σ_e^2 (5)	σ_w^2 (6)	σ_r^2 (7)
30″.....	12.36 ± 3.37	6.11 ± 1.11	6.25 ± 3.54	1.39 ± 0.43	0.33 ± 0.11	1.06 ± 0.44
60″.....	31.9 ± 18.0	16.3 ± 7.8	15.6 ± 19.6	2.1 ± 2.3	3.0 ± 1.0	-0.9 ± 2.5
80″.....	119 ± 72	34 ± 21	85 ± 75	24 ± 6	7 ± 2	17 ± 6

sources in our observed images, including the known nonlinear effects of the CLEAN algorithm (Anantharamaiah et al. 1991), source blending, noise bias, sidelobes, and the positive bias introduced by the 1.5 μJy "stumps" of bright sources (§ 2.3), will inherently be included in our simulations in the same way and the same level as those effects appear in our actual sky images. The techniques we employed to remove bright sources from our simulated sum images are described in § 2.3. We also constructed simulated difference images. We subtracted the variance observed in the difference images—essentially the noise put into the simulations—from the variance calculated in the simulated sum images using the techniques described in § 3.1. In the case of these simulations, the excess variance in the sum images is produced only by the randomly distributed radio sources in the field and their sidelobes.

We performed similar calculations for lower resolution, tapered images, in each case using the appropriate value for the instrumental and atmospheric noise as determined from the corresponding sky image. Each such simulation was repeated five times. The error in our estimate of the excess variance from these simulations is determined by combining in quadrature the statistical scatter between the simulations with the uncertainty introduced by the errors in slope and amplitude given in equation (5).

As we have noted above, the excess variance in the case of these simulations is in principle produced by the radio sources we have added to the simulations. There may be some small contribution from artifacts of the CLEAN process or other effects, but such additional contributions to the excess variance will be present in both the actual sky images and the simulated images. Thus, we take the excess variance calculated for the simulations as a reliable estimate of the variance introduced into our sky maps by weak sources and call it the *weak source variance*, σ_w^2. The values of σ_w^2 found from our simulations appear in Tables 5 and 6 (cols. [3], [6], and [9]).

We are now in a position to remove the effect of these weak sources to see if our sky images contain any additional, residual, variance. We do so by subtracting the weak source variance from the excess variance to obtain a quantity σ_r^2, the *residual variance.*

4. LIMITS ON CBR FLUCTUATIONS

We have collected in column (3) of Table 7 values for the residual variance in our sum images at various resolutions. In column (4), these values are converted to true sky variance as calculated from equation (3) using $\bar{P}^{-2}(\theta)$ as the conversion factor. If the residual sky variance is greater than zero, we may infer that there are fluctuations in the microwave sky above and beyond those produced by foreground radio sources and instrumental noise. We will generally ascribe all the residual variance to CBR fluctuations, thus producing the most conservative upper limits on $\Delta T/T$. Finally, 95% confidence upper limits on the sky variance were calculated as in Fomalont et al. (1993) by assuming σ^2 is a Gaussian variable. In that case, the 95% confidence level upper limit is the value of the sky variance σ^2 plus 1.645 times its standard error.

4.1. *Conversion to Brightness Temperature*

In the Rayleigh-Jeans region of a 2.726 K blackbody spectrum, the relation between $\Delta T/T$ and an observed variance σ^2 expressed in μJy^2 can be shown to be

$$\left(\frac{\Delta T}{T}\right) = 7.14 \times 10^{-3} \frac{(\sigma^2)^{1/2}}{\Omega}, \tag{6}$$

with $T = 2.726$ K (Mather et al. 1994) and Ω given in arcsec^2.

Since we based our analysis on *uncleaned* images constructed from data taken with two different array configurations, the solid angle Ω of the synthesized beam is not a well-defined Gaussian with $\Omega = 1.133\theta_{1/2}^2$. As a consequence, we measured the effective solid angle for each resolution by summing all the pixel intensities in the dirty beam, out to the first null of the beam. The resultant values for Ω are given in column (2) of Tables 7, 8, and 9, and we use them in equation (6) when calculating the $\Delta T/T$ limits appearing in the final column of Tables 7–9.

4.2. *Limits on Polarized CBR Fluctuations*

As in our earlier VLA work on linearly and circularly polarized fluctuations (Partridge et al. 1988; Fomalont et al. 1993), we also made images in Stokes parameters Q, U, and V and linear polarization maps constructed as $P = (Q^2 + U^2)^{1/2}$. Both tapered and full-resolution images were made. Since we expected that the *polarized* contribution from foreground sources would be minimal, we did not clean these polarized images or try in other ways to remove the polarized flux of foreground sources.

The angular dependence of the variance in the P, Q, U, and V images was analyzed in the same way as our total intensity sum map (§ 3.1). This analysis allows us to measure and subtract instrumental noise. The results for the V images are given in Table 8 in a format similar to that used in Tables 2–7. In this table and subsequent ones, if the variance is negative, we set it to zero in order to produce conservative upper limits on $\Delta T/T$. In Table 8, column (6),

TABLE 7

LIMITS TO CBR FLUCTUATIONS

Nominal Resolution (1)	Beam Solid Angle (arcsec^2) (2)	σ_r^2 (μJy^2) (3)	Sky Variance (μJy^2) (4)	$\Delta T/T$ ($\times 10^{-5}$) (5)	95% Confidence Level: Sky (μJy^2) (6)	95% Confidence Level: $\Delta T/T$ ($\times 10^{-5}$) (7)
6″.....	44.96	0.17 ± 0.20	0.22 ± 0.26	7.4 ± 8.1	<0.65	<12.8
10″.....	109.6	0.46 ± 0.48	0.59 ± 0.61	5.0 ± 5.1	<1.60	<8.2
18″.....	356	2.09 ± 1.87	2.68 ± 2.40	3.3 ± 3.1	<6.62	<5.2
30″.....	1096	6.25 ± 3.54	15.6 ± 8.9	2.6 ± 1.9	<30.2	<3.6
60″.....	3578	15.6 ± 19.6	39 ± 49	1.2 ± 1.4	<120	<2.2
80″.....	6736	85 ± 75	212 ± 188	1.5 ± 1.5	<521	<2.4

TABLE 8

LIMITS TO CBR FLUCTUATIONS: CIRCULARLY POLARIZED

NOMINAL RESOLUTION (1)	BEAM SOLID ANGLE (arcsec^2) (2)	σ_e^2 (μJy^2) (3)	SKY VARIANCE (μJy^2) (4)	95% CONFIDENCE LEVEL Sky (μJy^2) (5)	95% CONFIDENCE LEVEL $\Delta T/T$ ($\times 10^{-5}$) (6)
6″.....	44.96	0.04 ± 0.13	0.05 ± 0.17	<0.32	<9.0
10″.....	109.6	0.07 ± 0.28	0.09 ± 0.36	<0.67	<5.3
18″.....	356	-0.61 ± 0.81	-0.78 ± 1.04	<1.71	<2.6
30″.....	1096	-1.04 ± 1.62	-2.60 ± 4.04	<6.65	<1.7
60″.....	3578	7.0 ± 12.1	17.5 ± 30.3	<67.3	<1.6
80″.....	6736	42 ± 46	104 ± 116	<294	<1.8

we list the resulting 95% confidence level upper limits on circularly polarized fluctuations.

Since the P images were quadrature sums of two other images, they contain only positive values. Hence, random fluctuations will have Rayleigh distribution (Fomalont et al. 1993). If s is the standard deviation associated with a Rayleigh distribution defined as

$$R(x) = \frac{x}{s^2} \exp\left[-\frac{1}{2}\left(\frac{x}{s}\right)^2\right], \quad (7)$$

there is a 5% chance that a randomly chosen variable will exceed $2.45s$. For this distribution the rms scatter is $\sigma = 0.81s$. Thus, the 95% confidence level is set equal to $2.45s$ or $3.03\ \sigma$ for the linearly polarized images; these values are given in columns (5) and (6) of Table 9.

4.3. *Reliability of These Results*

At all resolutions, σ_r^2 is positive for Stokes I, total intensity images (though generally at the $1\ \sigma$ level or below), suggesting the presence of microwave sky variance in excess of that produced by random distribution of foreground sources obeying the source count relation (5). We now discuss a number of tests we perform to examine the reliability of these results, and of the consequent upper limits on CBR fluctuations.

First, we note that σ_e^2, and hence σ_r^2, remains positive even far from the center of our sum images, where $\overline{P^2}(\theta)$ tends to zero (see cols. [8]–[10] of Table 5). That suggests the possibility of a small, additional source of noise present in the sum images. For instance, at 6″ resolution, the variance in the outer regions of our sum images is $0.10 \pm 0.03\ \mu$Jy^2 higher than in the outer regions of the difference images. That is, the rms noise in the outer regions of the sum maps is 1.59 μJy, rather than 1.56 μJy. The corresponding figures for this additional variance in the 18″ and 60″ resolution maps are $0.73 \pm 0.17\ \mu$Jy^2 and $2.1 \pm 2.3\ \mu$Jy^2, respectively.

We have calculated the variance introduced by weak sources at distances $r > 200''$ from the image centers—see column (9) of Table 5 and column (6) of Table 6. Weak sources are evidently not responsible for the residual variance at $r > 200''$. We next investigate stronger sources which might be located in sidelobes of the primary beam of the VLA. While $\overline{P^2}(\theta)$ is small at $r \geq 200''$, it does not in fact go to zero, as assumed in § 3.1. $\overline{P^2}(\theta)$ can have values as large as 0.001 in sidelobes of the primary beam (Windhorst et al. 1993a). If we assume $\overline{P^2}(\theta) = 0.001$ at all $r > 200''$ throughout the image, and populate that region with sources obeying the relation (5), we find that up to half of the residual variance at $r > 200''$ can be explained. Some of the residual variance at $r > 200''$ may also be due to imperfect removal of the sidelobes of sources in the central 200″ of the images.

Whatever its cause, this additional noise in the outer region of our sum images is not solely responsible for the generally positive values of σ_r^2. For instance, at 6″ resolution, this additional noise contributes only $\sim 1/2$ of σ_r^2, and at larger scales, the contribution is even less ($\sim 1/4$ at 18″ resolution).

Next we ask whether our correction for the variation introduced by weak, foreground, radio sources could be in error, in the sense that σ_w^2 is underestimated from our extrapolations. Inspection of Tables 5 and 6 shows that σ_e^2 rises from ~ 1.3 to 3 times σ_w^2 as the resolution changes from 6″ to 80″; thus σ_w would need to be 20%–70% larger than we estimate in order to bring σ_r^2 to zero. An increase in σ_w of this magnitude would require a proportional increase in the

TABLE 9

LIMITS TO CBR FLUCTUATIONS: LINEARLY POLARIZED

NOMINAL RESOLUTION (1)	BEAM SOLID ANGLE (arcsec^2) (2)	σ_e^2 (μJy^2) (3)	SKY VARIANCE (μJy^2) (4)	95% CONFIDENCE LEVEL Sky (μJy^2) (5)	95% CONFIDENCE LEVEL $\Delta T/T$ ($\times 10^{-5}$) (6)
6″.....	44.96	-0.05 ± 0.06	-0.06 ± 0.07	<0.22	<7.4
10″.....	109.6	0.01 ± 0.12	0.01 ± 0.15	<0.47	<4.5
18″.....	356	0.07 ± 0.41	0.09 ± 0.52	<1.59	<2.5
30″.....	1096	0.05 ± 0.76	0.13 ± 1.91	<5.78	<1.6
60″.....	3578	-0.9 ± 3.8	-2.2 ± 9.4	<28.6	<1.1
80″.....	6736	-3.2 ± 11.7	-7.9 ± 29.3	<89	<1.0

coefficient of relation (5), or an abrupt change of slope from -1.2 to less than -1.4 at $S < 7$ μJy. The former is excluded by the source counts in Paper I, Donnelly, Partridge, & Windhorst (1987), Fomalont et al. (1991), and Windhorst et al. (1993a). The latter would present problems with the convergence of the source counts as S goes to zero. At some value of S, the slope must become less steep than -1.0 in the integral source counts to ensure that the brightness of the microwave sky does not diverge. Indeed, we have argued (Windhorst et al. 1993b) that the slope must be flatter than -1.0 at 0.02–0.1 μJy. It would be surprising, therefore, if the slope were to become steeper in the 0.1–7 μJy interval, only to flatten to -1.0 below 0.1 μJy. In addition, changing the slope of the source count law has only a small effect on σ_w on larger angular scales, where the residual variance is largest. For instance, for $\theta = 60''$, changing the slope to -1.4 increases our calculated value of the weak source variance by only a few percent.

Another way to increase σ_w^2 without altering the source count law is to assume that the sources are strongly clumped in position: σ_w^2 is proportional to the clumping factor C. While there is no evidence of clumping of bright radio sources, weaker, mJy, sources have been reported to be weakly clustered (Cress et al. 1996).

Finally, we note that one small region is responsible for a substantial contribution to the overall variance measured in the central 100″ or our image. This is a negative feature or "cool spot" approximately 25″ from the image center. This feature is visible in Figure 1*c* but is more prominent in tapered, lower resolution images. The reality of this feature, and the possibility that it is a Sunyaev-Zel'dovich signal from a distant cluster of galaxies, are discussed in more detail by Richards et al. (1997). Here, we assume the reality of this feature, and then examine the contribution it makes to the excess variance in the central regions of our sum images. We subtracted this negative feature from the map using the same method we employed to subtract bright positive sources from the map (§ 2.3). This allows us to set somewhat more stringent upper limits on the level of microwave fluctuations in the remaining portions of the central regions of our images (Table 10). At the finer resolutions ($\theta \leq 18''$), removing this single area of the map effectively reduces σ_r^2 to zero. Inspection of column (5) of Table 10 will show that removing this single area also results in a small decrease in our upper limits on $\Delta T/T$. For tapered images on larger angular scales, where we analyze the residual variance within the central 200″ of an image, the effect of removing the single feature is smaller (again, see Table 10).

Since the effect on our upper limits on $\Delta T/T$ of removing this negative feature in the map is not large, we will in general make use of the limits set in Table 7 when comparing our results to theoretical predictions. In any instance where we use the results from Table 10, we will make an explicit note of the fact that we are excluding a single negative feature from the analysis.

We can also calculate the effect of assuming a sharp cutoff in the radio source population below 7 μK. In the most extreme case, assuming there are *no* radio sources with $S < 7$ μK, σ_w^2 goes to zero. The effect on our upper limits on $\Delta T/T$ depends on θ: at 6″, our upper limit would double; by 60″ the increases would be only $\sim 15\%$.

5. INTERPRETATION OF RESULTS

At all resolutions, from 6″ to 80″, we find fluctuations in the microwave sky at approximately the 1 σ level, even after the effects of foreground radio sources have been removed. At resolutions $\theta \leq 18''$, much of the observed excess variance may be ascribed to a single negative feature, which we interpret elsewhere (Richards et al. 1996) as a possible Sunyaev-Zel'dovich signal from a distant cluster. At lower resolution, $\theta \geq 30''$, however, there remains marginal evidence for variance in the microwave sky beyond the calculated contribution of foreground sources. If we ascribe all of the sky variance to cosmic microwave background fluctuations, then we arrive at 95% confidence limits on $\Delta T/T$ of 12.8, 5.2, and 2.2×10^{-5} as the angular scale increases from 6″ to 18″ to 60″ (all from Table 7).

5.1. *Comparison with Previous Measurements*

We may compare the present results with our earlier work (Fomalont et al. 1993) on VLA observations at the same frequency and slightly poorer sensitivity. The results reported in the 1993 paper were based on D configuration observations only, so their angular resolution extends down only to 10″. The rms noise of the sum image at 10″ resolution was a factor of 2 higher in the earlier observations.

Nevertheless, the upper limits on $\Delta T/T$ we report here do not differ by a factor of 2 from those reported in the 1993 paper. Why is this so, given the greater integrating time and consequent lower noise in the present images? There are three reasons, two of them artifacts of the analysis of the data, and the third apparently connected with the microwave properties of the sky.

One reason why our new results do not compare more favorably to those of Fomalont et al. (1993) is that the

TABLE 10

EFFECT OF NEGATIVE FEATURE ON $\Delta T/T$ LIMITS

		Negative Feature Removed		
			95% Confidence Levels	
Nominal Resolution (1)	σ_r^2 from Table 7 (μJy^2) (2)	σ_r^2 (μJy^2) (3)	Sky (μJy^2) (4)	$\Delta T/T$ ($\times 10^{-5}$) (5)
6″.....	0.17 ± 0.20	-0.10 ± 0.19	<0.40	<10.0
10″.....	0.46 ± 0.48	-0.14 ± 0.43	<0.91	<6.2
18″.....	2.09 ± 1.87	0 ± 1.58	<3.33	<3.7
30″.....	6.25 ± 3.54	4.64 ± 3.34	<25.3	<3.3
60″.....	15.6 ± 19.6	21.6 ± 21.0	<140	<2.3
80″.....	85 ± 75	53 ± 65	<140	<2.1

actual synthesized beam size employed in the earlier work in some cases differed substantially from both the nominal FWHM listed in Tables 2–10 here and the beam size employed in the present work. The beam size, in turn, has an important bearing on calculations of $\Delta T/T$: for a fixed value of σ_r^2 in μJy^2, $\Delta T/T \propto \theta^{-2}$. For instance, in our present work, the nominal 10″ beam has a measured full-power beam width of 9.″8, whereas the beam width of the nominal 10″ beam in Fomalont et al. (1993) was closer to 13.″8. Thus, if we had comparable limits on σ_r^2, we would report an upper limit on $\Delta T/T$ almost 2 times larger here. As noted in § 4.1, the values of beam width we use in the present paper are closer approximations to the nominal values given in column (1) of Tables 2–10, so we use those in making our subsequent calculations.

The other change in the analysis of the data is the formula used to calculate the error in σ_e^2. In the present work, we used relation (4). Note that expression (4) assumes that the errors in σ_s^2 and σ_d^2 add in quadrature, whereas in our 1993 paper, we simply added the errors. In addition, we believe that the uncertainty in a variance like σ_s^2 is properly represented by $(2/N)^{1/2}\sigma_s^2$, which is $2^{1/2}$ larger than the value improperly used in our earlier work. Clearly, where the error in σ_s^2 dominates, the resulting error in σ_e^2 will be $2^{1/2}$ times larger than we would have estimated in 1993. In contrast, where Δ_d dominates, there will be little change. As a consequence, our values for σ_e^2 and, consequently σ_r^2 have errors ranging between 0% and 40% larger than they would have had we used the expression given in Fomalont et al. (1993). Since upper limits on $\Delta T/T$ depend on the error in the quantity σ_r^2, our upper limits on $\Delta T/T$ are again between 0% and 40% larger than they would have been using the 1993 formula for the error in σ_s^2.

In Table 11, we present the corrected upper limits derived from our earlier work (Fomalont et al. 1993) and combine them with the results in Table 7 to set overall constraints on $\Delta T/T$.

Finally, even after corrections have been made for instrument noise, bright foreground radio sources, weak foreground radio sources, a single negative region, and the slight excess noise in the sum images, there is some evidence of residual variation in the microwave sky, as was true in our earlier work. This residual signal is larger for lower resolution maps, but in no case is it clearly statistically significant. A positive value of σ_r^2 does, however, raise our upper limits on $\Delta T/T$ at all resolutions.

5.2. *Constraints on Models*

The upper limits on $\Delta T/T$ established here improve those determined by Fomalont et al. (1993) at angular scales $\geq 18''$ and reach to smaller angular scales as well. When these results and our earlier limits are combined, the resulting constraints on arcminute scales (col. [6] of Table 11) are comparable in sensitivity to measurements and upper limits on larger scales (e.g., the limit established on a $\sim 7'$ scale by Readhead et al. 1989: $\Delta T/T \leq 1.7 \times 10^{-5}$). We now use the results of Table 11 to provide constraints on theoretical models for CBR fluctuations on arcminute and subarcminute scales.

For instance, Loeb (1996) used our previous upper limit on $\Delta T/T$ at 18″ resolution to establish upper limits on the ultraviolet emissivity of Lyα clouds. Our new results lower the upper limit he established by 15% to $\langle J_{21}^2 \rangle^{1/2} \lesssim 10^{1.2 \pm 0.4}$.

We can also place constraints on models invoking cosmic strings for the production of large-scale structure (e.g., Stebbins et al. 1987; Bouchet et al. 1988; Moessner et al. 1994). Moessner et al. point out that the clearest test for the non-Gaussian fluctuations introduced by cosmic strings is the kurtosis k_4 in the distribution of temperature gradients. They give a formula for the kurtosis in terms of the beam scale θ, the horizon scale at last scattering θ_H, and a parameter M describing the density of the string network:

$$k_4 = 3 + \frac{0.14\theta_H}{M\theta}, \quad \text{or} \quad \sim 3 + \frac{16}{M\theta},$$

for θ in arcminutes. Moessner et al. (1994) evaluate this expression for the appropriate value $M = 10$, finding $k_4 \sim 8$ for their string model and $\theta = 18''$, versus $k_4 = 3$ for purely Gaussian fluctuations. This apparently clear discriminant between string and other models is greatly weakened, however, when we include the effects of instrumental noise (assuming instrument noise is itself Gaussian). Moessner et al. show that the kurtosis signature $(k_4 - 3)$ is reduced by a factor of 2 or more when the instrumental variance σ^2 exceeds $(\theta/11)\beta^2$, where β is a measure of the amplitude of the string signal:

$$\beta = 4\pi G\mu\gamma\left(\frac{v}{c^3}\right).$$

Here, μ is the mass/length of the cosmic string and v its transverse velocity. Strings are expected to move at rela-

TABLE 11

COMBINATION WITH EARLIER RESULTS[a]

	1993 RESULTS				
	As Published		Corrected		COMBINED 1993 + 1996
NOMINAL RESOLUTION (1)	σ_r^2, Sky (μJy)^2 (2)	$\Delta T/T$ Limit ($\times 10^{-5}$) (3)	σ_r^2, Sky (μJy^2) (4)	$\Delta T/T$ ($\times 10^{-5}$) (5)	LIMIT ($\times 10^{-5}$) (6)
6″.....	...	...	...	...	<12.8
10″.....	2.43 ± 2.18	<7.2	-0.3 ± 2.2[b]	<12.5	<7.9
18″.....	6.8 ± 8.5	<5.8	-4.2 ± 7.4[b]	<7.0	<4.8
30″.....	8.5 ± 22.5	<4.0	8.5 ± 27.2	<4.7	<3.5
60″.....	-28 ± 103	<2.3	-28 ± 129	<2.9	<2.0
80″.....	-153 ± 315	<2.1	-153 ± 340	<2.5	<2.1

[a] Fomalont et al. 1993.

[b] Converted to limits for inner 100″ only, using values of Ω from Table 7.

tivistic speed, so we take $\gamma v/c \sim 1$ and ask what range of μ would produce detectable kurtosis in our experimental results. At $\theta = 18''$ resolution, for instance, $\sigma \sim 3 \times 10^{-5}$, and we find that μ must exceed $\sim 2 \times 10^{23}$ g cm^{-1} to produce a clearly discernible kurtosis signal. Thus, the limits our work can place on string models are at the level of $\mu \sim 10^{23}$ g cm^{-1}.

A statistical analysis of this sort ignores the phase information in our images. We are investigating whether we can constrain the string parameters M and μ more tightly by looking directly for temperature steps in our images or by looking for non-Gaussian signatures in the *u-v* plane data (J. Maguejo 1996, private communication, 1996).

Bond, Carr, & Hogan (1991) have pointed out that the far-infrared thermal emission from high redshift galaxies can contribute substantially to the variance of the microwave sky at short wavelengths. Because the emission spectrum drops sharply with wavelength for such models, more useful constraints are set by the 3.4 mm anisotropy observations of Radford (1993) and by the constraints on spectral distortions established by the *COBE*–Far Infrared Absolute Spectrophotometer team (e.g., Mather et al. 1994).

Another source of microwave fluctuations, in this case independent of wavelength, is the nonlinear fluctuation introduced into the CBR if the universe is reionized (e.g., Vishniac 1987). As noted in the introduction, these fluctuations are referred to as *secondary* fluctuations, to distinguish them from those introduced at the epoch of recombination at $z \sim 1000$. Because of a self-canceling effect noted initially by Sunyaev (1978) and subsequently investigated by Kaiser (1984), ordinary linear perturbations in the density will not produce large-amplitude secondary fluctuations. But second-order effects can produce detectable signals, the most prominent of these being the so-called Vishniac effect, in which the temperature fluctuation is proportional to the product $\Delta\rho v$ (Vishniac 1987). Clearly, to estimate the amplitude of the Vishniac effect, one needs information about both density inhomogeneities and the velocity fields they induce. As a consequence, calculations of these secondary anisotropies are substantially more model-dependent than calculations of primary anisotropies. Both the amplitude and the angular scale of secondary anisotropies suffer from this model dependence. The angular scale, for instance, depends strongly on the cosmic density (e.g., Hu, Scott, & Silk 1994; Persi 1995), shifting to smaller scales as the density decreases. Nevertheless, for some models at least, upper limits on CBR fluctuations at a level of $1\text{–}3 \times 10^{-5}$ are beginning to provide useful constraints. As Hu et al. (1994) point out, baryon dark matter models with $\Omega_b \sim \Omega_0 \gtrsim 0.3$ violate the upper limits given here or by Subrahmanyan et al. (1993).

For some baryon-only models, predicted values of $\Delta T/T$ are much larger at $6''$ than at $60''$, for instance, 5–20 times larger for a particular model with $\Omega_b = 0.2$ and Hubble's constant = 80 km s^{-1} Mpc^{-1} (Hu et al. 1994). As it happens, however, our limits on $\Delta T/T$ at $6''$ are roughly 6 times less sensitive than at $60''$ (see Table 11), so our observations, despite their better angular resolution, do not improve the limits on the Vishniac effect already set by the Australia Telescope observations at arcminute scales (Subrahmanyan et al. 1993).

Although we have emphasized secondary fluctuations above, it is also true that the upper limits of Table 11 provide important data on primary fluctuations, those imprinted on the CBR at $z \sim 1000$. Our 95% confidence upper limits are a factor of ~ 2 lower than some robust detections of ΔT at the $\sim 1^\circ$ scale (e.g., Devlin et al. 1994; Ruhl et al. 1995; Netterfield et al. 1997). Thus our results (and those of Subrahmanyan et al. 1993) establish that the spectrum of CBR fluctuations does cut off at small scales (§ 1). That cutoff is expected at an angular scale of $\sim 7\Omega^{1/2}$. Thus, the determination of an approximate angular scale for the cutoff provides an estimate of the cosmological density parameter, Ω. Our upper limits suggest that $\Omega \gtrsim 0.1$, not yet a particularly critical constraint.

Finally, a number of groups (Korolev et al. 1986; Cole & Kaiser 1988; Schaeffer & Silk 1988; Markevitch et al. 1992, 1994) have noted that the inverse Compton scattering of CBR photons by hot gas in distant clusters of galaxies can introduce fluctuations into the microwave background. The mechanism is the Sunyaev & Zel'dovich (1972) effect. We have already noted that some of the residual variance we observe may be due to a single high redshift cluster in our image. In a separate paper, we investigate this possiblity further and also compare our observations with a network of models developed in the references cited above for the evolution of clusters of galaxies and their ionized gas content (Richards et al. 1997).

5.3. *Constraints on Galactic Microwave Emission*

Our values of $\Delta T/T$ (Table 7) have been corrected for atmospheric noise and the flux of discrete radio sources, but not for possible fluctuations in the Galactic foreground. At $\lambda = 3.6$ cm, synchrotron emission is expected to dominate the Galactic microwave foreground. Let us assume that our measured value on arcminute scales (Table 7), $\Delta T/T = (1.2 \pm 1.4) \times 10^{-5}$, is due to fluctuations in the surface brightness of Galactic synchrotron emission. Assuming a synchrotron spectral index of 0.7, then at $\lambda = 6$ cm we would expect $\Delta T/T$ fluctuations of amplitude:

$$\left(\frac{\Delta T}{T}\right)_6 \sim \left(\frac{6}{3.6}\right)^{2.7} (1.2 \pm 1.4) \times 10^{-5} \sim (5 \pm 6) \times 10^{-5}$$

on this same scale. In fact, the upper limit on fluctuations at this wavelength is 6×10^{-5} (Fomalont et al. 1988). Thus the possibility that our signal is Galactic is not yet ruled out by direct VLA observations. However, it would be surprising if there were variations in the synchrotron emission on the subparsec scales that $1'$ resolution implies.

We can, of course, turn the argument around and use our results and the earlier 6 cm observations to set 95% confidence upper limits on Galactic microwave fluctuations at centimeter wavelengths of roughly

$$(\Delta T/T)_s \lesssim (1.2 \times 10^{-6})\lambda^{2.7} ,$$

with λ in cm. If we ascribe all the fluctuations to thermal bremsstrahlung instead of synchrotron emission, the limit becomes

$$(\Delta T/T)_b \lesssim (2.7 \times 10^{-6})\lambda^{2.1} .$$

Work reported here was supported in part by a grant to the Northeast Astronomy Consortium from the William Keck Foundation and in larger part by NSF grant AST 93-20049 to Haverford College. R. A. W. acknowledges grant GO.2684.03.93A from STScI under contract with NASA. Jennifer Batty and Scot Harrison, both Haverford students, contributed substantially to the analysis of the data.

REFERENCES

Anantharamaih, K. R., Despande, A. A., Radhakrishnan, V., Ekers, R. D., & Goss, W. M. 1991, in IAU Symp. 131, Radio Interferometry: Theory, Techniques and Applications, ed. T. J. Cornwell & R. A. Perley (San Francisco: ASP), 6
Baars, J. W. M., Genzel, R., Pauliny-Toth, I. I. K., & Witzel, A. 1977, A&A, 61, 99
Banday, A. J., & Wolfendale, A. W. 1991, MNRAS, 252, 462
Birkinshaw, M., & Hughes, J. P. 1994, ApJ, 420, 33
Bond, J. R., Carr, B. J., & Hogan, C. 1991, ApJ, 367, 420
Bouchet, F. R., Bennett, D. P., & Stebbins, A. 1988, Nature, 335, 410
Brandt, W. N., Lawrence, C. R., Readhead, A. C. S., Pakianathan, J. N., & Fiola, T. M. 1994, ApJ, 424, 1
Carlstrom, J. E., Joy, M., & Grego, L. 1996a, ApJ, 456, L75
———. 1996b, ApJ, 461, L59
Colafrancesco, S., Mazzotta, P., Rephaeli, Y., & Vittorio, N. 1994, ApJ, 433, 454
Cole, S., & Kaiser, N. 1988, MNRAS, 233, 637
Cress, C. M., Helfand, D. J., Becker, R. H., Gregg, M. D., & White, R. L. 1996, ApJ, 473, 7
Delvin, M. J., et al. 1994, ApJ, 430, L1
Donnelly, R. H., Partridge, R. B., & Windhorst, R. A. 1987, ApJ, 321, 94
Fomalont, E. B., Windhorst, R. A., Kristian, J. A., & Kellermann, K. I. 1991, AJ, 102, 1258
Fomalont, E. B., Kellermann, K. I., Anderson, M. C., Weistrop, D., Wall, J. V., Windhorst, R. A., & Kristian, J. A. 1988, AJ, 96, 1187
Fomalont, E. B., Kellermann, K. I., Wall, J. V., & Weistrop, D. 1984, Science, 225, 23
Fomalont, E. B., Partridge, R. B., Lowenthal, J. D., & Windhorst, R. A. 1993, ApJ, 404, 8
Franceschini, A., Toffolatti, L., Danese, L., & De Zotti, G. 1989, ApJ, 344, 35
Grainge, K., Jones, M., Pooley, G., Saunders, R. Baker, J., Haynes, T., & Edge, A. 1996, MNRAS, 278, L17
Herbig, T., Lawrence, C. R., Readhead, A. C. S., & Gulkis, S. 1995, ApJ, 449, L5
Hindmarsh, M. 1993, ApJ, 431, 534
Hogan, C. J., & Partridge, R. B. 1988, ApJ, 341, L29
Hu, W., Scott, D., & Silk, J. 1994, Phys. Rev. D, 49, 648
Ikeuchi, S. 1981, PASJ, 33, 211
Kaiser, N. 1984, ApJ, 282, 374
Kellermann, K. I., Fomalont, E. B., Richards, E. A., Partridge, R. B., & Windhorst, R. A. 1996, in preparation (Paper I)
Knoke, J. E., Partridge, R. B., Ratner, M. I., & Shapiro, I. I. 1984, ApJ, 284, 479
Korolev, V. A., Sunyaev, R. A., & Yakubtsev, L. A. 1986, Soviet Astron. Lett., 12, 141
Kreysa, E., & Chini, R. 1989, in Third ESO/CERN Symposium, Astronomy, Cosmology and Fundamental Physics, ed. M. Caffo et al. (Dordrecht: Kluwer), 433
Loeb, A. 1996, ApJ, 459, L5
Makino, N., & Suto, Y. 1993, ApJ, 405, 1
Markevitch, M., Blumenthal, G. R., Forman, W., Jones, C., & Sunyaev, R. A. 1992, ApJ, 395, 326
———. 1994, ApJ, 426, 1
Martin, H. M., Partridge, R. B., & Rood, R. T. 1980, ApJ, 240, L79
Mather, J. C., et al. 1994, ApJ, 420, 439
Moessner, R. Perivolaropoulos, L., & Brandenberger, R. 1994, ApJ, 425, 365
Netterfield, C. B., Jarosik, N., Page, L., Wilkinson, D., & Wollack, E. J. 1997, ApJ, 474, 47
Ostriker, J. P., & Cowie, L. L. 1981, ApJ, 243, L127
Partridge, R. B. 1995, 3 K: The Cosmic Microwave Background (Cambridge: Cambridge Univ. Press)
Partridge, R. B., Nawakowski, J., & Martin, H. M. 1988, Nature, 311, 146
Persi, F. M. 1995, ApJ, 441, 1
Radford, S. J. E. 1993, ApJ, 404, L33
Readhead, A. C. S., Lawrence, C. R., Myers, S. T., Sargent, W. L. W., Hardebeck, H. E., & Moffet, A. T. 1989, ApJ, 346, 566
Rephaeli, Y. 1993, ApJ, 418, 1
———. 1995, ARA&A, 33, 541
Richards, E. A., Fomalont, E. B., Kellermann, K. I., Partridge, R. B., & Windhorst, R. A. 1997, AJ, in press
Ruhl, J. E., Dragovan, M., Platt, S. R., Kovoc, J., & Novak, G. 1995, ApJ, 453, L1
Schaeffer, R., & Silk, J. 1988, ApJ, 333, 509
Smoot, G. F., et al. 1992, ApJ, 396, L1
Stebbins, A., Veeraraghavan, S., Brandenberger, R., Silk, J., & Turok, N. 1987, ApJ, 322, 1
SubbaRao, M. U., Szalay, A. S., Schaefer, R. K., Gulkis, S., & von Groenefeld, P. 1994, ApJ, 420, 474
Subrahmanyan, R., Ekers, R. D., Sinclair, M., & Silk, J. 1993, MNRAS, 263, 416
Sunyaev, R. A. 1978, in IAU Symp. 79, The Large Scale Structure of the Universe, ed. M. S. Longair & J. Einasto (Dordrecht: Reidel), 393
Sunyaev, R. A., & Zel'dovich, Ya. B. 1972, Comments Astrophys. Space Sci., 4, 173
Tegmark, M., Silk, J., & Blanchard, A. 1994, ApJ, 420, 484
Vishniac, E. T. 1987, ApJ, 322, 597
Vittorio, N., & Silk, J. 1984, ApJ, 285, L39
White, M., Silk, J., & Scott, D. 1994, ARA&A, 32, 319
Wilbanks, T. M., Ade, P. A. R., Fischer, M. L., Holzapfel, W. L., & Lange, A. E. 1995, ApJ, 427, L75
Windhorst, R. A., Fomalont, E. B., Kellermann, K. I., Partridge, R. B., Richards, E., Franklin, B. E., Pascarelle, S. M., & Griffiths, R. E. 1995, Nature, 375, 471
Windhorst, R. A., Fomalont, E. B., Partridge, R. B., & Lowenthal, J. D. 1993a, ApJ, 405, 498
———. 1993b, in ASP Conf. Ser., Milano Symposium on Observational Cosmology, ed. G. Chincarini et al. (San Francisco: ASP), 534
Windhorst, R. A., Gordon, J. M., Pascarelle, S. M., Schmidtke, P. C., Keel, W. C., Burkey, J. M., & Dunlop, J. S. 1994, ApJ, 435, 577